

**A faster implementation of the hierarchical search algorithm for  
detection of gravitational waves from inspiraling compact binaries**

Anand S. Sengupta and Sanjeev Dhurandhar

*Inter-University Centre for Astronomy and Astrophysics,*

*Post Bag 4, Ganeshkhind, Pune 411007, India*

Albert Lazzarini

*LIGO Laboratory, California Institute of Technology,*

*MS 18-34, Pasadena, CA 91125, United States*

arXiv:gr-qc/0301025v1 8 Jan 2003

## Abstract

The first scientific runs of kilometer scale laser interferometric detectors like LIGO are underway. Data from these detectors will be used to look for signatures of gravitational waves (GW) from astrophysical objects like inspiraling neutron star/blackhole binaries using matched filtering. The computational resources required for online flat-search implementation of the matched filtering are large if searches are carried out for small total mass. Flat search is implemented by constructing a single discrete grid of densely populated template waveforms spanning the dynamical parameters - masses, spins - which are correlated with the interferometer data. The correlations over the kinematical parameters can be maximized apriori without constructing a template bank over them. Mohanty and Dhurandhar (1996) showed that a significant reduction in computational resources can be accomplished by using a hierarchy of such template banks where candidate events triggered by a sparsely populated grid is followed up by the regular, dense flat search grid. The estimated speed up in this method was a factor  $\sim 25$  over the flat search. In this paper we report an improved implementation of the hierarchical search, wherein we extend the domain of hierarchy to an extra dimension - namely the time of arrival of the signal in the bandwidth of the interferometer. This is accomplished by lowering the Nyquist sampling rate of the signal in the trigger stage. We show that this leads to further improvement in the efficiency of data analysis and speeds up the online computation by a factor of  $\sim 65 - 70$  over the flat search. We also take into account and discuss issues related to template placement, trigger thresholds and other peculiar problems that do not arise in earlier implementation schemes of the hierarchical search. We present simulation results for 2PN waveforms embedded in the noise expected for initial LIGO detectors.

PACS numbers: 04.80.Nn, 07.05.Kf, 95.55.Ym, 97.80.-d

## I. INTRODUCTION

Pulsar timing experiments by Hulse and Taylor [1, 2] led to accurate measurement of periastron time shifts in the PSR1913+16 binary pulsar system. These matched to the predictions from the theory of general relativity for energy losses due to gravitational waves (GW) to better than 0.5% accuracy. This was the first strong indirect evidence for the existence of GW. Over the last decade or so, a host of laser interferometric detectors like the two LIGO detectors [3] in USA, GEO600 in Germany [4], the TAMA 300 in Japan [5] and VIRGO in Italy-France [6] are being built to *catch* these waves *in flesh* and unravel the physics of the universe encoded in them. As of present, several of these interferometers are in advanced stage of completion. The TAMA 300 has achieved significant observation time with more than 1000 hours of observation whereas the LIGO had its first successful scientific run in August, 2002. Thus data from these detectors promise much interesting and new astronomical research over the next several years.

The most well studied sources of GW important to detection are compact astrophysical objects moving at relativistic speeds, like merging blackholes, spinning neutron star systems, inspiraling neutron star binaries etc. [7, 10]. A gravitational wave burst with a typical GW strain of  $h \sim 10^{-21}$  is expected to carry [8] about  $80 \times 10^{-6}$  watts/meter<sup>2</sup> past the modern detectors over a duration of  $\sim 10$  millisecc. However, GW interact so weakly with matter that even this huge flux of energy (by electromagnetic standards) will produce only a minute measurable signal of the above order in the arm lengths of the detectors. Detection of such weak signals requires special signal processing methods to extract the signature of these signals buried in the noisy output of these detectors.

Accurate waveform modeling of gravitational waves from the inspiral phase of compact binaries [9] makes it possible to look for their signatures using the technique of matched filtering and are considered to be the likely sources to be detected by the first generation of detectors. In the last few minutes of their inspiral, the frequency of the emitted GW will lie in the sensitive bandwidth of these detectors. Matched filtering involves cross correlating the detector output with a bank of template waveforms each having a different set of parameters. This is necessary since only the *form* of the expected signal is known and not its exact parameters *a priori*. Together, these templates span the whole range of parameters as determined from astrophysical considerations. This procedure is computationally less

efficient if implemented in a *flat* method which uses a very dense grid of templates to span the parameter space. The method is very well described in earlier literature - see [11–14] for example. A more efficient implementation of the flat search is desirable for several reasons. Eventually the interferometers will run continuously and real time analysis must be carried out in order to keep up with the data streams. This means that the time taken to analyze a data segment of duration  $T$  seconds, must be  $\leq T$  seconds in real time. By the same token, the computational efficiency of real time algorithms will limit the volume of the parameter space which one can search for GW signals in interferometer data. The desirability for the improved computational efficiency promised by the hierarchical algorithm presented here is twofold: (i) to date, there has been little or no optimization of the implementation of parallelized matched filtering algorithms and their performance will not scale with larger numbers of processors [16]; (ii) recent developments in the methodologies to handle more massive compact binary systems and to include non aligned spin have shown the need for a greater number of templates in a higher dimensional search space than has been applied in the first searches for lighter mass systems [23, 27].

A faster implementation of the matched filtering procedure was proposed by Mohanty and Dhurandhar [29, 30] which could reduce the computational cost of the search algorithm by a factor of 25 to 30 without sacrificing the efficiency of the flat-search method. It essentially involved using hierarchically staged analyses on two template grids instead of one dense grid. The first layer was that of trigger stage templates which were placed more sparsely than the second stage templates. Any *crossing* over the trigger threshold would be followed up *locally* by the fine bank. This trigger threshold must be carefully chosen such that not only could false alarms be kept in control, but also the detection probability of a genuine signal will be higher than a prescribed minimum (usually  $\sim 95\%$ ). The need for further improving upon the efficiency of implementing the matched filtering method is more pressing at present than ever - mainly because of our experience with real interferometer data over the recent past. Some of the benign assumptions which are used in prescribing the canonical search actually do not hold true in real time data - for example the stationarity and Gaussianity of interferometer noise is a key assumption to almost all the previous work. However, drifts in the noise power spectra and *tail* features therein severely undermine the efficiency of the matched filtering algorithm [19]. Thus hidden costs are incurred in carrying out even a flat search where  $\chi^2$  vetoing [17] is now prescribed to curb high unprecedented false alarm rates.

The TAMA data analysis team [18] had to put such vetoing even in the trigger stage of the hierarchical search. Such vetoing techniques add to the total cost of the online computational budget. An alternative implementation to the matched filtering has been proposed recently using the Fast Chirp Transform (FCT) method [20]. The complexity of this algorithm is comparable to that of the conventional matched filtering technique. It may become simpler under certain circumstances if it is possible to transpose the order in which the associated 2-D FFT is calculated. To date, however, this has not been explored further.

In this paper, we propose a faster implementation of the canonical hierarchical search method. Because most of the power in the chirp signal is at low frequencies - the power in the signal falls off as  $f^{-7/3}$  where  $f$  is the frequency - one can truncate the Fourier transformed data at a relatively lower frequency (we choose 256 Hz) and nonetheless retain sufficient signal power ( $\sim 92\%$ ) [24]. Then the key idea is to sample the data at a lower rate (512 Hz) in the trigger stage which gives us smaller FFT data sets to work upon. Lowering the first stage sampling rate also leads to a changed filter placement scenario where the absence of higher frequency modes of the GW chirp causes the ambiguity function to fall off more gradually and thus individual trigger templates can cover a bigger volume of the parameter space. This also leads to further computational advantage since the number of trigger templates is reduced. However, the lowered trigger thresholds and reduced signal to noise ratio due to this method will tend to increase the false alarm rate. We discuss these issues and supplement our solution with simulation results. In an earlier paper [24] we had outlined some of the above ideas. However, the scope of that paper did not include such complications as rotation of the parameter space, innermost stable circular orbit (ISCO) frequency cutoffs etc. Here, we take into account all these realistic scenarios to propose an extended hierarchical search (EHS) algorithm which can reduce the computational cost by a factor of  $\geq 65$  over a flat search. The family of restricted, spin-less 2PN family of chirp waveforms is used for our computation. We also use the target noise power spectral density of initial 4 km LIGO interferometers in our simulations [32].

## II. THE FLAT SEARCH

In this section, we at first gloss over the necessary background and notation in order to make the paper self contained. We then estimate the online computational cost of the

flat search. This will prepare us for the EHS and comparing the cost advantages thereof. Generic time domain functions  $h(t)$  will be denoted by  $\tilde{h}(f)$  in the Fourier domain, where

$$\tilde{h}(f) = \int_{-\infty}^{\infty} dt h(t) e^{2\pi i f t}. \quad (2.1)$$

Engineering and much of LIGO analysis software uses the opposite sign for the exponent in (2.1). We however maintain this notation for consistency with the published literature [19, 29].

### A. Matched filtering

The stationary phase approximated Fourier transform  $\tilde{h}(f)$  of the spin-less, restricted second post-Newtonian binary chirp is given up-to a constant factor  $\mathcal{N}$  by

$$\tilde{h}(f) = \mathcal{N} f^{-7/6} \exp i \left[ -\frac{\pi}{4} - \Phi_a + \Psi(f; M, \eta, t_a) \right], \quad (2.2)$$

where  $M = m_1 + m_2$  is the total mass of the binary system,  $m_1$  and  $m_2$  being the individual masses of the stars;  $\eta$  is the ratio of the reduced mass to the total mass;  $\Phi_a$  and  $t_a$  are respectively the arrival phase and the time when the frequency  $f$  attains the fiducial value  $f_a$ . The factor  $\mathcal{N}$  depends on the masses,  $f_a$  and the distance to the binaries. The function  $\Psi(f; M, \eta, t_a)$  describes the phase evolution of the inspiral waveform and is given by

$$\begin{aligned} \Psi(f; M, \eta, t_a) = & 2\pi f t_a + \frac{3}{128\eta} \left[ (\pi M f)^{-5/3} + \left( \frac{3715}{756} + \frac{55}{9}\eta \right) (\pi M f)^{-1} \right. \\ & \left. - 16\pi (\pi M f)^{-2/3} + \left( \frac{15293365}{508032} + \frac{27145}{504}\eta + \frac{3085}{72}\eta^2 \right) (\pi M f)^{-1/3} \right] \end{aligned} \quad (2.3)$$

It is important to distinguish between the nature of parameters that appear in the above *form* of the GW chirp. The two mass parameters  $\vec{\mu} \equiv \{M, \eta\}$  are the dynamical parameters and determine the *shape* of the chirp. Exclusive to this set are the ‘offset’ parameters  $\vec{\lambda} \equiv \{t_a, \Phi_a\}$  which determine the duration of the chirp or the end-points in the time series. The latter can be quickly estimated in the matched-filtering paradigm without having to construct template banks over them. For example, spectral correlators using FFTs allows us to estimate correlations at all time lags and thus estimate  $t_a$ . Similarly, using the quadrature formalism to construct template banks, the initial phase can be estimated analytically. However, the dynamical parameters need to be tackled by building a grid of templates which span them. In future, our parameter-space will refer explicitly to these mass parameters

unless otherwise mentioned. To ease the computation, a new set of time parameters  $\{\tau_0, \tau_3\}$  that are functions of the masses is chosen in which the metric defined over the parameter space is approximately constant. They are related to  $\{M, \eta\}$  by

$$\tau_0 = \frac{5}{256\pi\eta f_a} (\pi M f_a)^{-5/3}, \quad \tau_3 = \frac{1}{8\eta f_a} (\pi M f_a)^{-2/3}. \quad (2.4)$$

In other words, the template bank is set up over  $\vec{\mu} \equiv \{\tau_0, \tau_3\}$ . The form of (2.2) allows us to write the explicit quadrature representation of the  $i$ -th template as

$$\tilde{h}(f; \vec{\mu}_i, t_a, \Phi_a) = \tilde{h}_c(f; \vec{\mu}_i, t_a) \cos \Phi_a + \tilde{h}_s(f; \vec{\mu}_i, t_a) \sin \Phi_a, \quad (2.5)$$

where,

$$\begin{aligned} \tilde{h}_c(f; \vec{\mu}_i, t_a) &= i\tilde{h}_s(f; \vec{\mu}_i, t_a) \\ &= \mathcal{N} f^{-7/6} \exp i \left[ -\frac{\pi}{4} + \Psi(f; \vec{\mu}_i, t_0) \right]. \end{aligned} \quad (2.6)$$

The normalization constant  $\mathcal{N}$  in (2.5) is fixed by demanding unit norm of both  $h_c$  and  $h_s$  i.e.  $(h_c, h_c) = (h_s, h_s) = 1$ , where the scalar product  $(a, b)$  of two real functions  $a(t)$  and  $b(t)$  is defined as

$$(a, b) = 2 \int_{f_l}^{f_u} df \frac{\tilde{a}(f)\tilde{b}^*(f) + \text{c.c.}}{S_n(f)}, \quad (2.7)$$

where, we use the Hermitian property of Fourier transforms of real functions.  $S_n(f)$  is the one sided power spectral density of the noise of initial LIGO detectors [32]. Further,  $f_l \leq f \leq f_u$  is taken to be the effective spectral window for computing the scalar product. The lower frequency cut-off  $f_l$  is dependent on the sensitivity of the detector to seismic vibrations and is taken to be 30 Hz, whereas the upper frequency cut-off  $f_u$  is equal to half the full sampling frequency taken to be 2048 Hz in this paper. In practice, the upper cut-off frequency for the signal is held back from the Nyquist rate by a factor  $\sim 0.8$ . Therefore, for normalizing the templates, we choose an upper cut-off frequency  $f_c$  which is the minimum of 800 Hz and the so called ISCO cut-off frequency. The latter corresponds to the last stable circular orbit at which the inspiral phase is deemed to end and is relevant only for high masses when the ISCO frequency is less than 800 Hz. For low masses where the ISCO cut-off frequency is more than 800 Hz, the loss in SNR due to this band limiting is  $\sim 0.14\%$ , which is negligible.

Having thus set up a template bank, the statistic  $\rho$  for an output signal  $s(t)$  of the interferometer is the maximum of the signal to noise ratio (SNR) over all the templates

(labeled by  $i$ ) and the time-lags  $t_a$ . Thus, the statistic  $\rho$  is given [33] by,

$$\rho = \max_i \left[ \max_{t_a} \sqrt{(s, h_c)^2 + (s, h_s)^2} \right], \quad (2.8)$$

which is then compared with a pre-determined threshold  $\zeta$ . Any crossing above this threshold is recorded as a candidate event in flat search scenarios. Let the SNR be maximized by the  $\bar{i}$ -th template and at the time-lag  $\bar{t}_a$ . The phase offset of the chirp  $\Phi_a$  can then be calculated as:

$$\Phi_a = \tan^{-1} \left[ \frac{(s, h_s)}{(s, h_c)} \right]_{\bar{i}, \bar{t}_a}. \quad (2.9)$$

A detailed description of this procedure can be found in [11–14, 29].

## B. Computational cost of flat search

Since  $\vec{\mu}$  is spanned by a *discrete* grid of templates, it might so happen that a signal arriving at the interferometer has parameters that do not correspond to a grid point. In this event, the correlation of such a signal with the nearby templates will fall below the maximum obtainable value. The degree of discretisation is governed essentially by the rule of thumb - that in the worst case, the loss in correlation shall not exceed 3% of the maximum. This corresponds to a loss of event rate of roughly 10% which is an agreed upon number in the community. Given the range of masses which act as search limits and set the boundary of  $\vec{\mu}$ , a grid of templates is constructed with the above idea. The main computational cost incurred in the flat search method outlined previously is in performing the Fast Fourier Transforms (FFTs) and multiplying the elements. If a data segment of duration  $T$ , sampled over  $N$  points is parsed through a flat search, utilizing  $\mathcal{N}_t$  templates, the order of floating point operations is

$$\mathcal{N}_{\text{op}} \sim 6\mathcal{N}_t N \log_2(N). \quad (2.10)$$

If these many operations are to be carried out in real time, the computational speed in floating point operations per second (Flops) is given by

$$\mathcal{N}_{\text{flop}} = \frac{\mathcal{N}_{\text{op}}}{T_{\text{pad}}}, \quad (2.11)$$

where  $T_{\text{pad}}$  is the padding length in the data segment. Computationally it is advantageous to use stretches  $T$  that are significantly longer than the duration  $\sim 3 \times \Delta T_{\text{chirp}}$ , where  $\Delta T_{\text{chirp}}$



is the duration of the longest chirp. However, in order to preclude losing chirps that occur within  $\Delta T_{\text{chirp}}$  of the ends of the longer data stretch  $T$ , it is necessary to overlap adjacent epochs of data by this amount. Thus the effective computational time available to analyze a data stretch of duration  $T$  is  $T_{\text{pad}} = T - \Delta T_{\text{chirp}}$ .

For the mass range of  $1 M_{\odot} \leq M \leq 30 M_{\odot}$ , the longest chirp signal occurs when each of the component masses is equal to  $1 M_{\odot}$ , and is  $\sim 95$  sec in duration. The data segments are taken to be 512 sec each (greater than three times  $\Delta T_{\text{chirp}}$ ), so  $T_{\text{pad}} \sim 417$  sec. The parameter spaces for the individual mass ranges of  $1 M_{\odot} \leq M \leq 30 M_{\odot}$  and  $0.5 M_{\odot} \leq M \leq 30 M_{\odot}$  in the  $\{\tau_0, \tau_3\}$  coordinates are shown in Fig. 1.

The mass range is set to  $1 M_{\odot} \leq M \leq 30 M_{\odot}$  in this paper and is typical for the initial detectors. The lower mass limit is chosen relatively higher, because higher masses lead to higher SNR (the SNR scales as  $M^{5/6}$ ), in order to compensate for the relatively lower sensitivity expected for the initial detectors. Choosing the fiducial frequency  $f_a = 40$  Hz, the area of the parameter space is  $8.5 \text{ sec}^2$ . If the parameter space is covered by a rectangular lattice of templates, obtained by using the largest inscribed rectangle within the contour of 3% mismatch, the density of templates is  $\sim 1300 / \text{sec}^2$ . Multiplying the density by the area gives about  $\mathcal{N}_t = 11,050$  templates which are needed to cover the parameter space. One typically takes 512 sec data trains sampled at 2048 Hz which gives  $N = 2^{20}$ . With a padding length of  $T_{\text{pad}} \sim 417$  sec and using Eq. (2.10, 2.11), we see that the online Flop rating required is  $\sim 3.2$  G-Flops. In addition to the cost of FFTs, there are overhead costs, incurred in element by element multiplication of the data and template vectors and data preprocessing. However, we neglect them in our analysis since they are small compared to the FFT costs.

The above estimate however does not take into account boundary effects, where the templates can spill out of the searched parameter space because of imperfect tiling. This effect can considerably increase the number of templates. The current LIGO template placement code [14] was run for the above parameters and was found to generate almost three times as many templates as in this simple estimate. Since the current code sets the fiducial frequency equal to the lower cut-off frequency,  $f_a$  was set at 30 Hz for the purpose of obtaining the number of templates.

Lowering the mass limit, increases the area of the parameter space and thus the computational cost. The results are described in Table I.

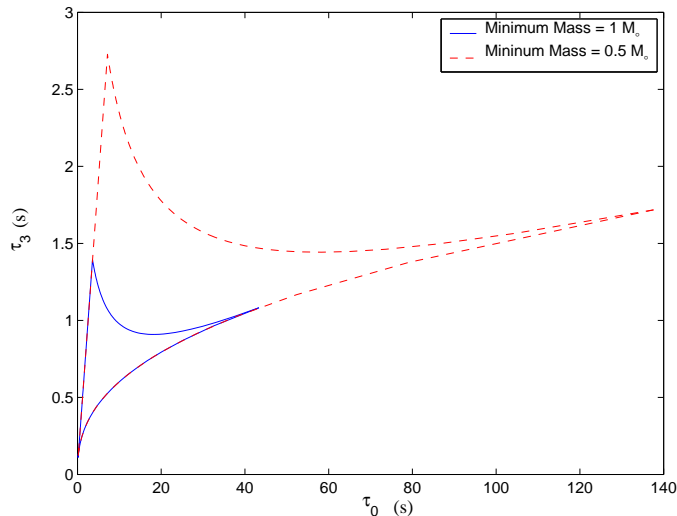


FIG. 1: Parameter spaces for the individual mass ranges  $1 - 30 M_{\odot}$  (solid line) and  $0.5 - 30 M_{\odot}$  (broken line) in  $(\tau_0, \tau_3)$  co-ordinates with  $f_a = 40$  Hz. Note that the  $\tau_0$  should be multiplied by  $(f_a/f_l)^{8/3}$  in order to get the Newtonian chirp time.

TABLE I: Estimates of number of templates and online computational cost for flat search. Templates are placed using the method prescribed by Owen and Sathyaprakash [26]. The prescribed minimum mismatch level is set at 0.97. The area of the parameter space is computed for the fiducial frequency of  $f_a = 30$  Hz. The upper mass limit in all the cases is set to  $30 M_{\odot}$ .

Minimum Mass Limit	Area <sup>a</sup> (sec <sup>2</sup> )	$\mathcal{N}_t$	$\mathcal{N}_{\text{flop}}$ (G-Flops)
$1.0M_{\odot}$	29.3	$3.34 \times 10^4$	10.1
$0.5M_{\odot}$	172.9	$1.64 \times 10^5$	49.5
$0.2M_{\odot}$	1687.4	$1.16 \times 10^6$	350.0

<sup>a</sup>The area of the parameter space scales as  $f_a^{-13/3}$ .

As mentioned before, the template placement code presently implemented employs effectively a rectangular tiling method. We note here that if a hexagonal closed packing method were used instead, significant reduction in the online computational speed can be accomplished, because of the efficiency of this method in covering the parameter space is greater

than rectangular packing [21, 24, 31]. As a matter of fact, the hexagonal tiling method gives a template density which is about  $\sim 25\%$  less, thus effectively reducing the required online computational speed by the same factor.

### III. EXTENDED HIERARCHICAL SEARCH

The flat search described in the previous section is not computationally optimal. This is due to the fact that a grid of large number of templates is required in order to densely span  $\vec{\mu}$ , satisfying the criterion that the minimal correlation for two neighboring normalized templates does not fall below a prescribed value of 0.97.

It turns out that we can significantly reduce the computational cost by constructing two sequential grids of varying template densities instead of one [29, 30]. The philosophy behind this approach is the fact that one expects real events to be not only weak but also very rare. This implies that most of the time, one is only spending time in sifting through interferometer noise. In this sense, scanning the parameter space so thoroughly at each observational epoch is wasteful. On the contrary, if a trigger mechanism exists which would pick up only statistically likely candidates, then a higher parameter resolution search (flat search) can be performed *locally* on pre-screened candidates possibly containing a chirp event. Thus figuratively, the hierarchical search method is a layered search. The coarse bank layer is the trigger which flags a likely event. This is then followed up by the fine grid of templates *a la* flat search method described above. The difference is that only a few fine grid templates can accomplish the job of thoroughly verifying the claim of the trigger stage coarse grid templates. The computational cost thus is reduced as fewer templates are employed in the overall scheme.

The above idea can be extended even further to include the time of arrival of the signal in the overall scheme of hierarchy as we shall now explain. From (2.2), one notices that the signal power spectrum is a decreasing power law in frequency :

$$|\tilde{h}(f)|^2 \propto f^{-7/3}. \quad (3.1)$$

From (3.1), we see that most of the signal power is contributed from the lower frequency bands. An immediate consequence is that one can cut off the chirp at a lower cut-off frequency and re-sample it at a lower Nyquist rate without losing too much power in the

signal. In the EHS we propose to sample the trigger stage data train at a much lower sampling rate than that used in a flat search algorithm. As a proof of principle, we notice that the fractional signal to noise ratio  $\rho$  as a function of an arbitrary upper cut-off frequency  $f_{\text{cut-off}}$  is given by  $\rho(f_{\text{cut-off}}) = I(f_{\text{cut-off}})/I(f_c)$ , where

$$I(f_{\text{cut-off}}) = 2 \int_{f_l}^{f_{\text{cut-off}}} \frac{df}{f^{7/3} S_n(f)}, \quad f_l < f_{\text{cut-off}} \leq f_c. \quad (3.2)$$

If the ISCO cut-off is used,  $f_{\text{cut-off}}$  must be replaced by the appropriate plunge cut-off frequency. However, this is applicable for high masses in the first stage ( $M \geq 16 M_\odot$ ), which is a tiny fraction of the parameter space - implying a negligible effect on the overall gain factor. A significant fraction of the SNR can be recovered from a relatively small value of  $f_{\text{cut-off}}$ . Specifically, for  $f_{\text{cut-off}} = 256$  Hz, (i.e. a sampling rate of  $f_{\text{samp}}^{(1)} = 512$  Hz) almost 92% of the signal power is recovered. The most obvious advantage of lowering the Nyquist rate in the first stage is that we have to contend with fewer points in computing the FFTs, (the cost of which scales as  $N \log_2 N$ ), leading to a reduction in first stage computational cost. For example, a chirp cut-off at  $f_{\text{cut-off}} = 256$  Hz reduces the cost of FFT by almost a factor of 4.

The equation (3.2) correctly estimates the loss in SNR if the time of arrival parameter  $t_a$  of the signal coincides exactly with a sampled time in the time-series. If, as will be the case in general,  $t_a$  is not a sampled time, then there will be an additional loss of SNR due to mismatch in time of arrival parameter. Considering the ‘worst case’ scenario when  $t_a$  of the signal lies exactly between two consecutive time samples, we numerically estimated this additional loss in SNR in two different cases : (a) when the chirp times of the signal match exactly with those of a template and (b) when they lie exactly in between two neighboring templates. In the former case, we found that the additional loss in SNR is less than 5% and in the latter case, a little more than 2%. It is to be noted however, that our template placement schema (see Sec III C) introduces some overlap between neighboring templates, which effectively reduces the maximum mismatch. We find that this adequately compensates for the additional loss in SNR and no further reduction of first stage threshold (prescribed in Sec IV A) is necessary.

In the earlier method given by Mohanty and Dhurandhar [29], the hierarchy was on the two mass parameters alone in the sense that a coarse template bank spanning the mass parameters was used as the trigger, followed up by a fine template bank. Analogously in the

EHS algorithm, we not only retain this hierarchy of templates spanning the mass parameters but also extend it to the time of arrival by coarser sampling of the signal at the trigger stage. It is in this sense that the EHS should be thought of as a three dimensional hierarchical search.

But quite aside from this, lowering the Nyquist rate also affects the contours of the ambiguity function  $\mathcal{H}$  which in turn affect the template coverage in the first stage. Also a lowered signal power in the first stage will require lowering the trigger threshold. This will affect the false alarm rate due to noise in the interferometer and in turn the overall computational cost. In the next few subsections, we systematically address these issues and prescribe the optimum method of implementing the EHS algorithm.

### A. Setting up the fine bank

In this subsection, we will discuss the setting up of the fine bank templates and the second stage threshold.

The templates in the second stage or the fine bank stage of the EHS is set up in a way that is identical to the flat search method discussed in the earlier section. The ambiguity function  $\mathcal{H}$  centered at the  $\vec{\mu}$  is defined as the correlation between two neighboring normalized templates whose mass parameters differ by  $\Delta\vec{\mu}$ :

$$\mathcal{H}(\vec{\mu}, \Delta\vec{\mu}) = \max_{t_0} \left( \tilde{h}(\vec{\mu}, \vec{\lambda}), \tilde{h}(\vec{\mu} + \Delta\vec{\mu}, \vec{\lambda}) \right). \quad (3.3)$$

The contours of  $\mathcal{H}$  are closed curves and the area enclosed within this curve will be frequently referred to as a *tile*. The shape of this tile depends on the contour level  $\Gamma$  where  $0 < \Gamma < 1$ . For values of  $\Gamma$  close to 1, the tiles are elliptical in shape. However, as  $\Gamma$  significantly differs from unity, the shape can be quite irregular. This is important from the point of view of template placement where the parameter space must be efficiently covered by these tiles. In the fine bank, the templates are laid out in such a way that nowhere does  $\Gamma$  fall below 0.97. For such high values of  $\Gamma$ , the ambiguity function can be approximated quite well by a Taylor expansion of  $\mathcal{H}$  truncated after the quadratic term. This allows analytic calculation of the dimensions of these elliptical tiles and placement of templates [25, 26] over  $\vec{\mu}$ . This is not true, however, for smaller values of the match level. The number of templates indirectly affect the minimum observable signal strength in the second stage of the hierarchical search

method and thus the overall minimum detectable signal strength.

In order to proceed with the numerical analysis, the noise in the interferometers is assumed to be a stationary, zero-mean Gaussian random process. Thus the integrated signal to noise ratio  $\rho$  calculated using (2.8) should also be considered to be a realization of a random process whose probability distribution depends on the presence or absence of the signal. In the presence of a signal, the distribution is a Rician, whereas in the absence of the signal,  $\rho$  is Raleigh distributed. The detection strategy is to set a threshold  $\zeta$  such that given one instance of  $\rho$ , a decision can be made with some statistical significance, whether or not, it was drawn from a Raleigh or a Rice distribution - which would correspondingly imply the presence or absence of a GW signal.

Given a sufficiently high  $\zeta_2$  (in the second stage), even in the absence of a signal, there may be some crossings of  $\rho$  above this value leading us to incorrectly deduce the presence of a signal. This threshold is thus primarily set such that the probability of these false alarms is no more than once per year. Thus,  $\zeta_2$  is set at

$$\zeta_2 = \sqrt{2 \ln(\epsilon \mathcal{N}_t^{(2)} T_{\text{yr}} f_{\text{samp}})}, \quad (3.4)$$

where, the data train is sampled at  $f_{\text{samp}}$  Hz and  $T_{\text{yr}} = 3.15 \times 10^7$  are the seconds in a year. The factor  $\epsilon$  arises from the correlation between templates and correlations between successive time-lags in the filtered output [28]. Because the chirp filter is a narrow band filter and band-passes the data, the inverse Fourier transformed data in the time domain becomes correlated as it is essentially generated from few frequency bins. Thus  $\epsilon$  gives the fraction of the number of independent Gaussian random variables in the total filter bank output. From our simulations we find that  $\epsilon \sim 0.6$  in the second stage where the templates are closely spaced, and  $\epsilon \sim 0.9$  in the first stage where the templates are farther apart. If there had been no correlation between the templates, we could have set  $\epsilon = 1$ . Using Eq.(3.4), and the fact that the sampling frequency in the second stage is 2048 Hz, we find that the second stage threshold must be put at  $\zeta_2 = 8.2$ . If this threshold coincides with the strength of minimum observable signal  $S_{\text{obs}}$ , then the detection probability is just 50%. In order to achieve higher detection probability, the minimum observed strength of the signal should be somewhat greater than  $\zeta_2$ . Following [30], we compute the detection probability by considering the joint probability of two neighboring templates around the signal. Then for attaining a minimum of 95% detection probability, the minimum strength of the signal

should be  $S_{\text{obs}} = \zeta_2 + \Delta\zeta$  where  $\Delta\zeta \sim 0.7$ . The second stage templates can thus detect a signal of strength  $S_{\text{obs}} = 8.9$  with a detection probability of 95% or greater. From the minimum match that we have chosen (97%), we see that this corresponds to a signal of minimum strength  $S_{\text{min}} = 9.2$  arriving at the detector.

## B. Setting up the trigger stage templates

The data trains in the trigger stage of the extended hierarchical search are sampled at 512 Hz, and the template chirps are terminated at 256 Hz, so as to avoid power aliasing effects in the FFTs. These templates are used as triggers. The neighborhood of a trigger is then searched using the second stage fine bank templates.

We begin by describing the contours of  $\mathcal{H}$  when the GW chirp is cut-off at a lower frequency, i.e. when  $f_{\text{cut-off}} = 256$  Hz. The contours at different  $\Gamma$  levels are not only irregular in shape, but cover larger tile areas compared to those with cut-off  $f_{\text{cut-off}} = 800$  Hz. The basic reason for the irregular shape of tiles is that, the higher order post-Newtonian (PN) terms that appear in the phase function  $\Psi$  in Eq. (2.3) decay slowly with the frequency  $f$ . The phase function  $\Psi$  appears implicitly in the integral of the ambiguity function. While the Newtonian term (the  $\tau_0$  term) falls off as  $f^{-5/3}$ , the  $\tau_2, \tau_3, \tau_4$  (1 PN, 1.5 PN, 2 PN) terms fall off as  $f^{-1}, f^{-2/3}, f^{-1/3}$  respectively. The 1.5 PN and 2 PN terms contribute to the phase significantly at high frequencies since their fall off is relatively slower. Thus an upper cut-off of 256 Hz versus 1024 Hz produces tiles that differ significantly in shape. The irregular and asymmetric shape of the contour can also be viewed as an effect of the curvature of the manifold. Because the 2 PN or the  $\tau_4$  term has not decayed, it contributes to the metric making it non-constant in the  $\{\tau_0, \tau_3\}$  space. The bigger tiles are essentially due to the fact that, it is the higher frequencies which resolve between the masses, and if these are cut off, the ambiguity function decays more gradually, resulting in bigger tiles. At  $\Gamma \sim 0.8$  the tiles with  $f_{\text{cut-off}} = 256$  Hz are larger in area than those with  $f_{\text{cut-off}} = 800$  Hz by about a factor of 2. Moreover, because the contours are large, non-local effects are important, compounding the curvature effects and adding to the irregular shape of the contour.

In the earlier hierarchical scheme, the ambiguity function in both the trigger and fine bank stages were the same. The trigger stage templates were constructed by letting the trigger threshold drop from  $\zeta_2$  to a lower value  $\zeta_1$  such that a balance was struck between

the following opposing forces :  $\zeta_1$  was low enough to allow larger tiles to cover the parameter space with fewer templates and thus reduce the computational cost, but high enough so that false alarm crossings due to noise do not compromise the cost advantage by increasing the second stage cost. Signal power in the trigger stage was the same as in the fine bank stage since the sampling rate was the same in both stages.

In the EHS implementation of the hierarchical search, we are faced with a different proposition - we have reduced signal power in the first stage due to lower cut-off frequency. Also, we have a different  $\mathcal{H}$  in the two stages. Given these differences, we need to devise how to set up the coarse grid of templates. We now describe the template placement for the first stage of the EHS algorithm.

### C. Setting up the trigger stage tiles

The tiling problem stated from an operational point of view is the following : given the prescribed match level  $\Gamma$  for the trigger stage, we need to tile the parameter space *efficiently* with closed contours of  $\mathcal{H}$ . The following conditions must be satisfied [31] for efficient template placement: firstly, minimal mismatch must be satisfied *i.e.*  $\mathcal{H} \geq \Gamma$  inside and on the contour. Also, templates should be placed such that there are no uncovered spaces (no holes) and there is minimal overlap between templates. For computational ease, the templates should preferably lie on a regular grid or at least a piece-wise regular grid. As stated earlier, the ambiguity function  $\mathcal{H}$  is quite wide at low frequency cut-offs since the mass resolution is poor in absence of high frequency components. We choose  $\Gamma = 0.8$  contours in the trigger stage to tile the available parameter space, since the total cost is minimum for this value of  $\Gamma$ . The results quoted at the end of the paper are also for other values of  $\Gamma$  but close to 0.8. It is quite unwieldy to use these contours *prima facie* to tile the parameter space. A possible solution is to carve a regular polygon - e.g. a rectangle out of these contours and use them as tiling blocks. To minimize the computational cost, we must choose the rectangle as large as possible. The details of a template placement (tiling) algorithm are now described. The demands made upon the tiling algorithm are several - (i) given a  $\Gamma = 0.8$  contour centered at some point in the parameter space, the largest rectangle should be identified *automatically* and used as the representative tile at that point, (ii) having placed a template at a point in the  $(\tau_0, \tau_3)$  space, the optimum position of



the neighboring templates should be estimated such that the template placement conditions are satisfied, and lastly (iii) the parameter space in  $(\tau_0, \tau_3)$  co-ordinates has non-trivial curvature because of which the contours are asymmetric and also have differential rotation as a function of  $(\tau_0, \tau_3)$  and one cannot set up a global regular grid for arbitrary values of  $\Gamma$ . The tiling scheme should correct for these differential rotations so that there are no uncovered spaces due to differential rotation of the rectangular tiles. The description of this tiling algorithm proceeds in the following logical sequence - we first describe a method of carving a large rectangle given a contour of  $\mathcal{H}$  at a specified value of  $\Gamma$ . Thereafter a method for placing neighboring templates is described. This method automatically takes into account the differential rotation of the templates. Finally, an overall placement schema is given which involves ‘stacking’.

The steps involved in identifying a sufficiently large rectangle given a  $\Gamma = 0.8$  contour is illustrated using one centered at  $(\tau_0 = 15.0 \text{ sec}, \tau_3 = 0.88 \text{ sec})$ . The rectangle must align itself along the length of the contour. So the first step is to identify the orientation of the rectangle. This is done by fitting straight lines to the concave sides of the contour with respect to the center. The points are so chosen that it also includes the one which is radially closest to the center as can be seen in Fig 2(a). If the slopes of these two lines are  $\tan \theta_1$  and  $\tan \theta_2$  respectively, then the side of the rectangle is chosen to have the average slope  $\tan \theta$ :

$$\tan \theta = \frac{1}{2}(\tan \theta_1 + \tan \theta_2). \quad (3.5)$$

The next step involves drawing two parallel lines with their slope  $\tan \theta$ , such that they (a) are as far out as possible from the center (b) intersect the contour at only two points (c) lie completely inside the contour. This is clearly shown in Fig 2(b) where the intersection points are labeled as A,B,C and D.

Two adjustable parameters are used to fix the distance of each side of the rectangle from the center of the contour. These parameters should be chosen such that conditions given above are satisfied. Due to the peculiar shape of the contour, the lines (see Fig 2(b)) may intersect the contour at multiple points. This must be avoided by fine tuning the parameters.

The final step is to read off the co-ordinates of the rectangle by dropping suitable perpendiculars. This is shown in Fig 2(c), and the resultant rectangle is shaded. In general, if the axes are scaled differently, the rectangles would look like parallelograms.

By following the above steps, a sufficiently large rectangle can be identified from within

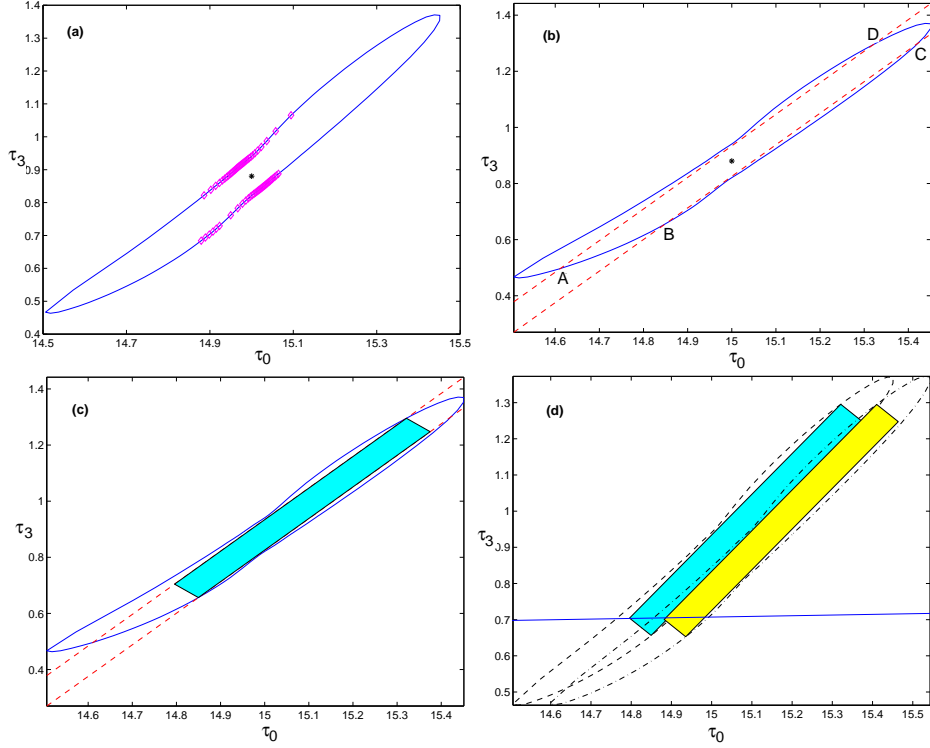


FIG. 2: This figure illustrates the sequential steps for obtaining the inscribed rectangle and placing the templates. Units of  $\tau_0$  and  $\tau_3$  are in seconds. (a) The orientation of the rectangle is first determined by fitting straight lines to points around the concave sides of the contour. (b) Then lines with slope  $m = \tan \theta$  are drawn inside the contour on either side. These intersect at four points A,B,C,D. (c) The rectangle is then extracted from the four points by dropping perpendiculars. (d) Figure illustrating the placement of two neighboring templates along some curve  $f(\tau_0, \tau_3) = 0$  parallel to the  $\eta = 1/4$  line. Note the slight overlap between the templates due to  $\Delta\theta = 0.025$  correction and the negligible spillage of rectangle below the equal mass line.

any prescribed contour. Before placing neighboring templates, one needs to correct for the differential rotation of the templates. This is achieved with an adjustable angular parameter  $\Delta\theta$  in the schema which deliberately induces some overlap between nearest neighbor templates by reducing the *effective* length and breadth of the rectangle that is used. If the actual dimensions of the rectangle are  $l$  and  $b$ , the  $\Delta\theta$ -corrected values  $l'$  and  $b'$  are given by

$$b' = l \tan \left[ \tan^{-1} \left( \frac{b}{l} \right) - \Delta\theta \right], \quad (3.6)$$

$$l' = b \tan \left[ \tan^{-1} \left( \frac{l}{b} \right) - \Delta\theta \right]. \quad (3.7)$$

The parameter  $\Delta\theta$  should be chosen very carefully so that minimal overlap condition is satisfied. The curves in Fig 3(a) show the overlap fraction between neighboring rectangles

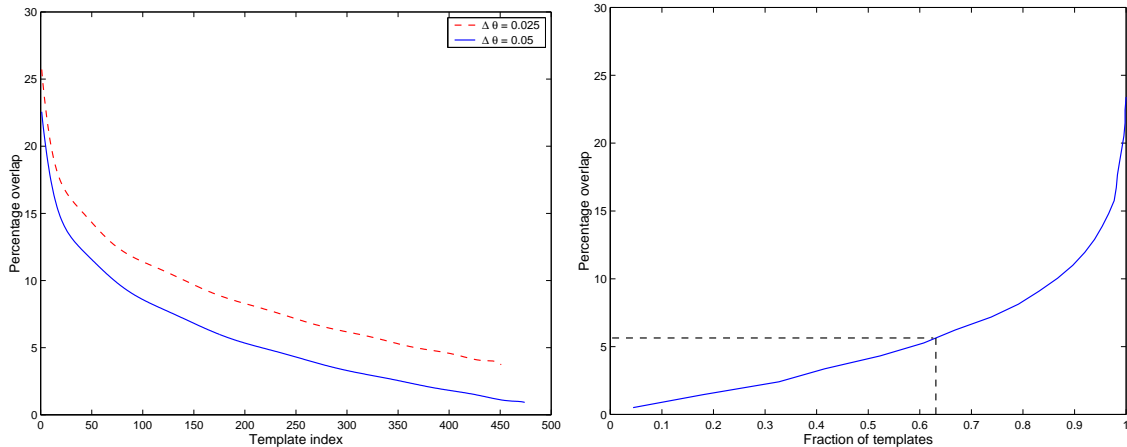


FIG. 3: (a) Percentage overlap between neighboring templates after  $\Delta\theta$ -correction. The values are  $\Delta\theta = 0.025$  (top) and  $\Delta\theta = 0.05$  (bottom). Percentage overlap is defined as the ratio of area common to two neighboring templates to the area of any one of them expressed as a percentage. Note that fewer templates are required for smaller  $\Delta\theta$  parameters. (b) Cumulative distribution of templates according to the  $\Delta\theta$ -induced area overlaps between neighbors for  $\Delta\theta = 0.025$ . The average percentage overlap in this case is 5.7%. The dotted line shows that  $\sim 63\%$  of the templates have percentage overlaps less than this average value.

as we move along the  $\tau_0$  axis for  $\Delta\theta = 0.05$  and  $\Delta\theta = 0.025$  respectively. We need to tweak the parameters such that the overlap approaches zero as quickly as possible without ever going below it. This will guarantee a minimum number of templates. Fig. 3(b) shows that for  $\Delta\theta = 0.025$ , most of the templates have neighboring overlaps of  $\sim 5\%$  of their width.

One would like to place the templates along some curve  $f(\tau_0, \tau_3) = 0$ . For example, this curve could be the equal mass line ( $\eta = 1/4$ ). Once the curve is chosen, the center of the neighboring template is found by moving out by a distance  $\Delta\tau_0$  along the  $\tau_0$  axis given by

$$\Delta\tau_0 = b' \frac{\cos \beta}{\sin(\theta - \beta)}, \quad (3.8)$$

where,  $b'$  is the  $\Delta\theta$ -corrected breadth and the local slope of the curve  $f(\tau_0, \tau_3) = 0$  is  $\tan \beta$ . For the  $\eta = 1/4$  line ( $m_1 = m_2$ ), the slope can be analytically determined :

$$\tan \beta = \frac{d\tau_3/dM}{d\tau_0/dM},$$

$$= \frac{64}{25} \pi^2 f_a M, \quad (3.9)$$

where  $2 M_\odot \leq M \leq 60 M_\odot$  is the total mass of the compact binary system. The  $\tau_0$  co-ordinate of the center of the new rectangle is given by  $\tau_0 + \Delta\tau_0$ . The  $\tau_3$  co-ordinate can be found from the equation of the curve.

This is a *dynamic* method of placing the templates. However, we do not go to such lengths in placing the neighbors. Since the average orientation of the rectangle is known, a constant fudge-factor in multiplying  $b'$  is quite sufficient. In this case, one relies entirely on the dynamical change in  $b'$  across the parameter space. Choosing  $\Delta\tau_0 \simeq 1.28b'$  is sufficient for our purposes. This choice will slightly increase the first stage cost. The placement of two neighboring templates is shown in Figure 2(d). Note that the overlap between the rectangles is small.

Our overall strategy of template placement is to build *stacks* of templates as can be seen in Fig 4. Here it is worth noting that all earlier schemes [13, 31] start by placing templates on the equal mass ( $\eta = 1/4$ ) line. However, the space below this line is unphysical - as such, almost 50% of the templates centered on this line will be wasted and the final result is that we end up using too many of first stage templates in covering the parameter space. We can ensure more efficient coverage by constructing templates on a line parallel to the  $\eta = 1/4$  line but which is offset by parameters  $\ell_p$  and  $\theta$  as :

$$\tau_0 = \tau_{0,\eta=1/4} + \ell_p \cos \theta, \quad (3.10)$$

$$\tau_3 = \tau_{3,\eta=1/4} + \ell_p \sin \theta, \quad (3.11)$$

where  $\ell_p$  is so chosen that the rectangle constructed spills minimally below the equal mass line. Due to the asymmetry of the contour,  $\ell_p$  need not be equal to half the length of the inscribed rectangle.

By shifting up the templates in this way, a larger area of the parameter space is covered than if their centers were placed on the equal mass line. Even though one needs to place templates all along the curve for the first stack - for the subsequent stack, templates need to be placed only between points of intersection of the top of the templates of the earlier stack with the parameter space boundaries  $m_1 = M_{\max}$  and  $m_1 = M_{\min}$ . Thus the first stack completely covers the low mass end of the parameter space from  $\tau_0 \gtrsim 7$  sec. Also the high mass end of the parameter space,  $\tau_0 \lesssim 2$ sec is covered by the first stack. Having placed

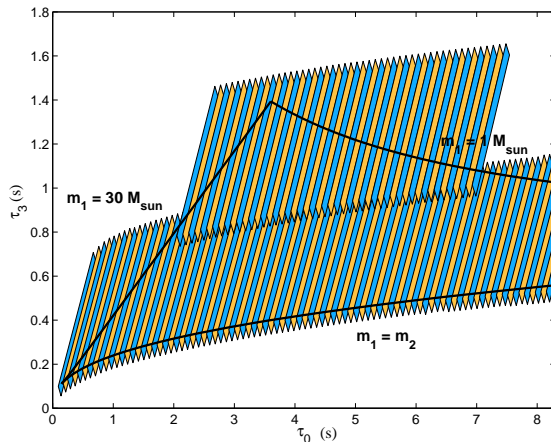


FIG. 4: Figure illustrating the stacks of templates on top of each other covering a part of the targeted parameter space. The dark lines are the boundaries of the parameter space for the mass range  $1 M_{\odot} \leq m_1, m_2 \leq 30 M_{\odot}$ . Due to the large size of the rectangles, the hierarchical search will actually cover more of the parameter space than the flat search it replaces. Note that this figure is a zoomed view of the first 20% of the  $\tau_0$  domain.

the first stack of templates in this way, the next stack is constructed by choosing the curve that is parallel to the first stack, but offset further according to the sizes of the templates in the previous stacks and adjusted for minimal overlap. The two stacks completely cover the parameter space. We find that the total number of coarse templates required is  $\mathcal{N}_t^{(1)} \sim 510$  for the contour level of  $\Gamma = 0.8$ .

If the lower mass limit had been smaller, say,  $0.5 M_{\odot}$ , then more than two stacks would have been required. It is easy to see how this schema can be generalized for smaller component masses. The details of placement using the above scheme towards the high mass end of the parameter space is shown in Figure 4.

The template placement schema described above *stacks* rectangular templates centered on curves parallel to the equal mass line, and the size of each tile covers a significant portion of the parameter space  $\vec{\mu}$ . As such, it is important that the length of templates in any stack does not vary too much. Indeed, the length of these tiles is seen to change by only a few percent over  $\vec{\mu}$ . However their orientations change by  $\sim 0.1$  radians and is seen to be a dominant effect at the high mass end. The parameter  $\Delta\theta$  takes care of this in our schema by introducing extra overlaps between neighboring templates. We thus find that the issue of varying template sizes is less of a concern than varying orientation of the templates.

This completes the formal description of the template placement algorithm.

#### D. Simulation of EHS

We performed Monte Carlo simulations to check the performance of the EHS algorithm against simulated detector noise with injected signals at different positions in the parameter space.

Only the trigger stage of the EHS is of relevance in this context since, the flat search used locally around a candidate event in the second stage is quite efficient in extracting relevant signals. The purpose of these simulations was to ascertain if the noise crossings were as expected as used in the analysis and design phase of the EHS algorithm. Secondly, since template placement method used in the first stage does not center the tiles on the  $\eta = 1/4$  line, we would like to check how efficiently signals with parameters close to this line are triggered by the first stage templates.

We chose a bank of  $\mathcal{N}_t^{(1)} = 11$  trigger stage templates covering the fraction of the parameter space where the ambiguity function is non zero. For ease of discussion, we label these from  $T_1$  to  $T_{11}$  (see Figure 6). The simulation was carried out in two phases. In the first phase we parsed data segments of 512 sec duration containing only simulated Gaussian stationary noise with LIGO-I power spectral density through these templates. In the second phase, a chirp signal with a predetermined maximum SNR  $\rho$  was added to the noise. The trigger stage sampling rate was chosen to be 512 Hz, such that the number of points in each data segment in this stage was  $N_1 = 2^{18}$ . The spectral window for this stage is taken to be  $30 \text{ Hz} \leq f \leq 256 \text{ Hz}$ .

The noise in the interferometers is assumed to be a Gaussian, whose characteristics remain constant in time. We used the LIGO-I noise spectral density to color samples of white Gaussian noise. From (2.8), one notices that in presence of noise only, the filtered SNR from each of  $\mathcal{N}_t^{(1)} = 11$  templates is expected to be realizations of a random process with Raleigh distribution. As remarked earlier in the context of fine bank placement, the filtered output from each of the templates is correlated. We account for this fact by introducing the quantity  $0 < \epsilon < 1$ , which is used to reduce the effective number of independent random variables. Using these, one can calculate the probability of the test statistic crossing a preset threshold  $\zeta_1$ . This is precisely the false alarm probability  $Q_0(\mathcal{N}_t^{(1)}, \zeta_1)$  as a function of the

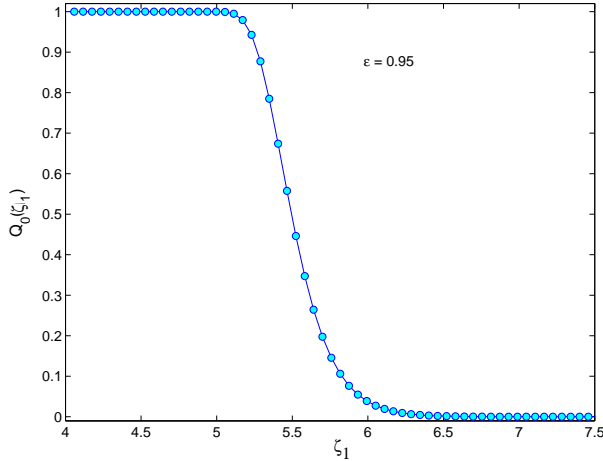


FIG. 5: False alarm probability estimates as a function of the first stage threshold for  $N_T = 11$  templates. The solid curve is obtained from (3.12) with  $\epsilon = 0.95$ , whereas the solid circles are the Monte Carlo estimates.

number of templates used and the first stage threshold. Assuming Gaussian noise, it can be expressed as

$$Q_0(\mathcal{N}_t^{(1)}, \zeta_1) = 1 - \exp[\epsilon \mathcal{N}_t^{(1)} N_{\text{pad}} \exp(-\frac{\zeta_1^2}{2})], \quad (3.12)$$

where  $N_{\text{pad}} = T_{\text{pad}} \times f_{\text{samp}}^{(1)}$  is the number of points in the non-overlapping segments of adjacent analysis epoch,  $T_{\text{pad}}$ . This curve is then compared with the result obtained from simulations and  $\epsilon$  is chosen to make the analytical expression agree with the Monte Carlo results. The parameter  $\epsilon$  should be taken as a measure of the statistical independence of the templates;  $\epsilon = 1$  means all the  $\mathcal{N}_t^{(1)} N_{\text{pad}}$  random variables are independent. In Figure 5, we have plotted the Monte-Carlo estimates of the false alarm probability. For the trigger stage of the EHS, where the distances between templates are quite large, we expect the assumption of statistical independence to hold to a large extent. Indeed, the best fit parameters for the curve gives  $\epsilon \simeq 0.95$ .

In the next phase of simulations, we added known signals to interferometer noise realizations and processed the data through eleven templates.

We chose our signal parameters at three characteristic positions in the parameter space with respect to the centers of the templates such that they represented three different detection scenarios. In case (A), the signal parameters were chosen to be favorably placed with respect to the filters. This was done by taking a point close to the center of  $T_6$  (see discussion in caption of Fig 6). In case (B), we chose the signal to have parameters such

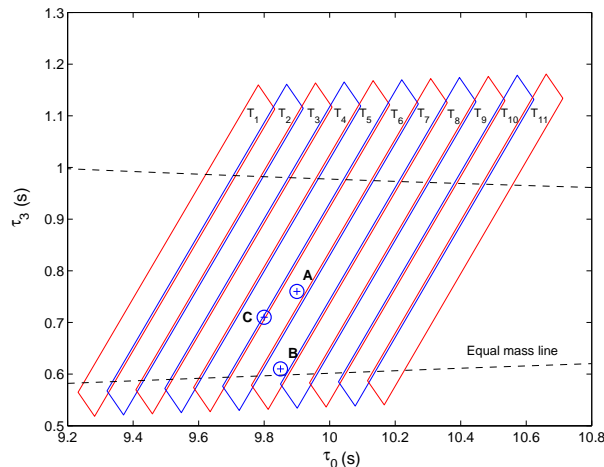


FIG. 6: The positions of  $\mathcal{N}_t^{(1)} = 11$  templates used in the simulation and the relative positions of the signals injected into the interferometer noise. The templates are labeled  $T_1$  to  $T_{11}$ . See the text for a description of the three simulation cases A, B and C.

TABLE II: Monte Carlo estimates of detection probability and percentage of triggers generated by individual  $N_T = 11$  templates in three different cases : (A) signal lies on  $T_6$  and close to template center (B) signal parameters lie on  $T_7$  and are quite far away from the center of the templates. Actually in this case the parameters lie close to the equal mass line. (C) The parameters lie exactly between  $T_5$  and  $T_6$ , and close to the equal mass line. The templates are individually labeled from  $T_1$  to  $T_{11}$ .

Case	$Q_d(\%)$	$T_1$	$T_2$	$T_3$	$T_4$	$T_5$	$T_6$	$T_7$	$T_8$	$T_9$	$T_{10}$	$T_{11}$
A	99.1	0.0	0.0	0.0	0.0	0.3	99.2	0.5	0.0	0.0	0.0	0.0
B	97.2	0.0	0.0	0.0	0.0	0.0	0.0	90.0	9.9	0.1	0.0	0.0
C	95.7	0.0	0.0	0.0	0.2	53.9	44.3	1.2	0.2	0.2	0.0	0.0
Noise	3.7	0.3	0.7	0.3	0.3	0.3	0.2	0.2	0.5	0.2	0.2	0.5

that it lay in the area bounded by  $T_7$ , but placed far away from the template centers - close to the equal mass line. In case (C), the signal was chosen to lie close to the equal mass line, exactly between  $T_5$  and  $T_6$ . We believe that these scenarios are typical for templates placed anywhere in the  $(\tau_0, \tau_3)$  parameter space, as it is more or less flat.

When only noise was processed, the trigger stage extended hierarchical search templates



registered on an average 0.3% false alarm probability per template. However we found that these alarms were isolated events in the sense that they were not triggered by multiple adjacent templates in unison. On the contrary when a bona fide signal was present, there were always a cluster of nearby templates which showed crossings above the trigger stage threshold. For the purposes of this paper, we choose the crossing with the maximum SNR for determining the trigger template; that is we select just *one* template in a given realization of the interferometer noise. This is like a one point estimate of the signal parameters when multiple trigger templates have shown crossings. The Monte Carlo simulation described below justifies this approach.

The results of this phase of the Monte Carlo simulation are summarized in Table II. In absence of a signal, we find that all the templates are equally likely to register a false alarm, the probability of which is in agreement with (3.12). In presence of a genuine signal, one notices that when the overlap between the signal and templates is high (case A), the signal is almost always correctly triggered (by  $T_6$ ). When the distance between the signal and templates is large (case B) then there is significant loss in correlation. In this case, we notice that about 10% of the triggers *spill over* to the adjacent templates. Finally, when the signal lies exactly between two templates (case C), the triggers are equally distributed between the adjacent templates.

Given these results, we can draw a strategy for chalking out the area over which the local flat search needs to be carried out in the second stage around every first stage trigger template. We introduce a factor  $\alpha$  which quantifies this idea.  $\alpha$  is the ratio of the area of the parameter space searched in the second stage for a given click to the area of the first stage template. Thus,  $\alpha = 1$  means the fine bank search is carried out within an area of the first stage template. But as the simulations show we need to search beyond this region with the fine bank, and thus  $\alpha$  needs to be chosen greater than unity in most of the parameter space. The parameter space boundaries can however make  $\alpha < 1$  especially at the low mass end where the parameter space tapers and very little area within the parameter space is required to be searched. Below we quote the value of  $\alpha$  averaged over the entire parameter space. If the interferometer noise is adequately described by a Gaussian random process, then our simulations bear out that searching two adjacent templates around the clicked template(s) should account for the correct location of the signal to  $< 1\%$  error. Thus it is sufficient to set  $\alpha = 2.5$ .

In presence of non-Gaussian features in the interferometer noise, the behavior of triggers can be quite unpredictable and we anticipate formidable difficulties in choosing the neighborhood for the fine search. Strategy based on the actual noise behavior will have to be devised. More work needs to be done towards a robust estimation of signal parameters from the trigger stage output itself so that the cost of the second stage can be minimized.

#### IV. COMPUTATIONAL COST OF EHS ALGORITHM

The computational cost in the EHS algorithm comes from (a) processing the data segment through all the first stage trigger templates, (b) a fine bank search in the neighborhood of all the triggers generated in (a) above and (c) cost of preprocessing and passing putative events between coarse and fine banks of the hierarchical search. In the cost analysis, we do not consider (c). However, we pause to note that if (c) is sufficiently large, it can completely nullify the gains we claim the extended hierarchical search method makes over a flat search. It maybe possible to setup the problem such that in the worst case, it is no worse than a flat search.

Let a data segment of  $T$  sec duration be sampled at  $f_{\text{samp}}^{(1)}$  Hz in the first stage and  $f_{\text{samp}}^{(2)}$  Hz in the second stage. The total floating point operations performed in the first stage is given by

$$\mathcal{N}_{\text{op}}^{(1)} \simeq \mathcal{N}_{\text{t}}^{(1)} (6f_{\text{samp}}^{(1)} T \log_2(f_{\text{samp}}^{(1)} T)), \quad (4.1)$$

where,  $\mathcal{N}_{\text{t}}^{(1)}$  is the total number of first stage templates employed. Furthermore, the frequency of triggers generated in (a) depends on the first stage trigger threshold  $\zeta_1$ . As we shall see later,  $\zeta_1 \simeq 6.05$  is the optimum first stage threshold. This corresponds to the optimum size of first stage tiles at  $\Gamma \simeq 0.82$  contour level, which gives us  $\mathcal{N}_{\text{t}}^{(1)} = 560$  in this stage. If such a threshold is put, the average number of crossings  $\bar{n}_c$  due to noise alone (assumed Gaussian and stationary ) is given by

$$\bar{n}_c \sim \mathcal{N}_{\text{t}}^{(1)} Q_0(1, \zeta_1), \quad (4.2)$$

where  $Q_0(1, \zeta_1)$  is the false alarm probability for a single template and is given by,

$$Q_0(1, \zeta_1) = 1 - \exp[\epsilon N_p \exp(-\frac{\zeta_1^2}{2})], \quad (4.3)$$

where  $\epsilon \simeq .95$  was the value obtained from the simulations which we mentioned in the previous section.

From this false alarm probability, the second stage floating point operations coming only from false alarms is estimated to be,

$$\mathcal{N}_{\text{op}}^{(2)} = \bar{n}_c \alpha \gamma \left( 6 f_{\text{samp}}^{(2)} T \log_2(f_{\text{samp}}^{(2)} T) \right), \quad (4.4)$$

where  $\gamma = \mathcal{N}_{\text{t}}^{(2)}/\mathcal{N}_{\text{t}}^{(1)}$  is the ratio of the number of templates in the second stage to the number of templates in the first stage, and  $\alpha\gamma$  is the number of fine bank templates required to search the neighborhood of the trigger template that clicks. The Monte Carlo results indicate that  $\alpha = 2.5$  should be sufficient. We round this up to the integer value 3. Estimates of the computational cost and the speed-up factor over the flat search for these values of  $\alpha$  are tabulated in Table III. The computational cost estimates make the plausible assumption that the analysis will be dominated by the need to dismiss false alarms, rather than processing true events. Therefore, the computational cost incurred when a signal is actually present in the data segment is not considered in these estimates. In our analysis, we have considered the second stage cost to be given by Eq. (4.4).

The online computational power for the two stages can be calculated by dividing the number of floating point operations  $\mathcal{N}_{\text{op}}^{(m)}$ ,  $m = 1, 2$  by the processed (zero-padded) length of the data segment  $T_{\text{pad}}$ :

$$\mathcal{N}_{\text{flop}}^{(m)} = \frac{\mathcal{N}_{\text{op}}^{(m)}}{T_{\text{pad}}}. \quad (4.5)$$

The total online speed  $\mathcal{N}_{\text{flop}}^{(\text{tot})}$  is the sum of the two online speed for the two stages:

$$\mathcal{N}_{\text{flop}}^{(\text{tot})} = \mathcal{N}_{\text{flop}}^{(1)} + \mathcal{N}_{\text{flop}}^{(2)}. \quad (4.6)$$

### A. Choosing the optimal $\zeta_1$

We consider data segments of 512 sec duration which accommodate chirps of maximum length 95 sec with sufficient padding corresponding to a minimum mass limit of  $1.0 M_{\odot}$ . We consider first and second stage sampling frequencies of 512 Hz and 2048 Hz respectively. The cutoff frequency for the chirp in the first stage is set at  $f_{\text{cut-off}} = 256$  Hz. Thus the number of data points to be processed are  $2^{18}$  and  $2^{20}$  for the coarse and fine banks respectively. The signals of minimal strength that can be observed, assuming a minimum detection probability of 95% and 3% mismatch between templates turns out to be 9.17 [29]. The first stage  $S_{\text{min}}$  for the above mentioned cut-off can be calculated to be 92% of 9.17 which is 8.44. If we choose

a mismatch level of  $\Gamma$  in order to tile the templates, the minimum  $S_{\text{obs}}$  seen by each template will be  $8.44 \times \Gamma$ . The first stage trigger level  $\zeta_1$  must be chosen at approximately  $8.44 \times \Gamma - 0.7$  so that the detection probability exceeds 95% even in this stage. As discussed in [29], although minimum detection probabilities of 95% are chosen at each stage of the hierarchical search, the true detection probability is still  $\sim 95\%$  because of the strong correlation among the statistics of the first and second stages.

For relatively low values of  $\Gamma$ , the size of each individual rectangle is very large, so that fewer templates suffice to cover the parameter space. However, since  $\zeta_1$  is also reduced in the process, there will be far too many crossings due to noise (false alarms) each of which need to be followed up by the fine bank *i.e.* second stage filters. Thus the second stage cost increases. On the other hand, when  $\Gamma$  is high, the area covered by individual first stage tiles will be quite small, and therefore a larger number of tiles are needed to cover the parameter space thereby increasing the first stage cost.

At some optimum value of  $\Gamma = \Gamma_{\text{opt}}$ , the total cost reaches a minimum. This is the optimum contour level for laying the first stage templates. The optimum contour level also determines corresponding optimum value of the trigger threshold  $\zeta_1$ . From Fig 7, we find that  $\Gamma_{\text{opt}} \sim 0.8$ .

TABLE III: Estimates of the computational cost for the two stage EHS algorithm and gain factors over the one step flat search algorithm.  $\Gamma$  is the contour level of the ambiguity function used to lay the trigger tiles. The speed-up factor  $\mathcal{G}$  is defined as the ratio of required online computational cost for the flat search to  $\mathcal{N}_{\text{flop}}^{(\text{tot})}$ . The online flat search cost is estimated to be  $\sim 3.2$  G-Flops.

	$\mathcal{N}_t^{(1)}$	$\bar{n}_c$	$\mathcal{N}_{\text{flop}}^{(1)}$	$\mathcal{N}_{\text{flop}}^{(2)}$	$\mathcal{N}_{\text{flop}}^{(\text{tot})}$	$\mathcal{G}$
$\alpha = 2.5$ $\Gamma = 0.81$	535	0.82	36.3	11.7	48.0	64
$\Gamma = 0.82$	564	0.51	38.3	6.8	45.1	68
$\alpha = 3.0$ $\Gamma = 0.81$	535	0.82	36.3	14.0	50.3	61
$\Gamma = 0.82$	564	0.52	38.3	8.4	46.7	66

Using the above formulae, we are now in a position to estimate the online computational cost of the EHS. Recall that for the mass range considered, the longest chirp signal occurs for the smallest component masses  $m_1 = m_2 = 1 M_{\odot}$ . For the lower cut-off of  $f_l = 30$  Hz

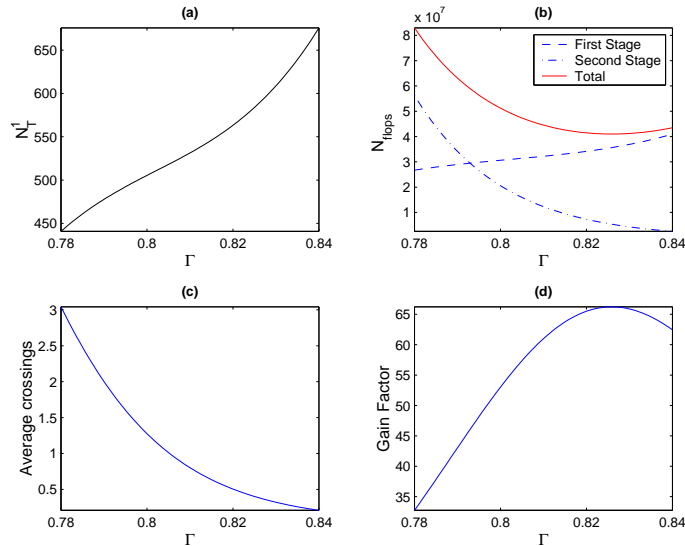


FIG. 7: (a) Number of trigger templates plotted against  $\Gamma$ . (b) Online cost of EHS algorithm plotted against  $\Gamma$ . (c) The average number of crossings in the first stage. (d) The speed-up factor  $\mathcal{G}$  factor defined as ratio of online flat search cost to online total EHS cost is plotted against  $\Gamma$ . As the contour level  $\Gamma$  is increased, the first stage cost increases because more trigger templates are required, while the second stage cost goes down because the false alarm rate goes down. The total cost is minimum at an optimum value  $\Gamma_{\text{opt}} \sim 0.8$  where the speed-up factor is maximum.

this signal is about 95 sec. Thus  $T_{\text{pad}} \sim 512 - 95 = 417$  sec. In the description of the flat search we mentioned that a total of  $\mathcal{N}_t = 11,050$  templates were required. Furthermore, implementing the trigger stage template placement method described above, we find that a total of  $\mathcal{N}_t^{(1)} = 564$  templates would be required in this stage. Finally, setting  $\zeta_1 = 6.05$  and using (4.2 - 4.6) we have  $\mathcal{N}_{\text{flop}}^{(\text{tot})} = 45.1$  M-Flops. This should be compared with the cost of a flat search given in Table I. For the similar mass limit, we find that the EHS algorithm reduces the online computational cost requirement over a flat search by a factor of  $\sim 68$ . The results for various choices of the parameters  $\alpha$  and  $\Gamma$  are summarised in Table III.

## V. CONCLUSION

We have investigated the performance of a new implementation of the two-step hierarchical search algorithm for detection of gravitational waves from compact inspiraling binaries where the first stage is coarsely sampled in time, while retaining the earlier flavor of hierar-

chy of templates over the mass parameters. The noise power spectral density used in this work is that of the initial LIGO. We have described a new method of placing templates in the trigger stage of the hierarchical search. We have also clearly outlined methods to set up thresholds at the two levels based on probability arguments.

The calculation of false alarm probabilities and detection probabilities in this paper follow from a basic assumption of Gaussianity and wide sense stationarity of the noise in the gravitational wave detectors. Also, we have assumed statistical independence of the output from the templates. However, we are aware that this may not be the case when the templates are placed closely. We have performed Monte Carlo simulations to verify the effect of statistical correlations between the templates. Our simulations show that there is very little correlation between the processed output of the first stage templates. We believe that this is because of the fact that in this stage the template separations are quite large compared to earlier implementations of the hierarchical search. We also find that even when the signal parameters are far away from the template centers, there is no appreciable loss in detection probability. This result is however obtained for Gaussian noise. We estimate that an optimum implementation of the EHS algorithm would reduce the required online computing power by a factor of 65 – 70 over a flat search. The *shape* of the noise power spectral density has an important bearing in the calculation of these numbers.

If most of the compact binaries are likely to have equal companion masses, templates centered on the  $\eta = 1/4$  line will pick them up with a higher detection probability. But this entails using greater number of first stage templates since a significant fraction of these templates would spill over into the unphysical part of the parameter space - below the  $\eta = 1/4$  line. We have adopted a different strategy wherein we have tried to minimize this template spillage. Our simulations show that even when the signal parameters lie close to the equal mass line, there is no appreciable loss in detection probability. However, to improve the probability of detection in the scheme, templates can be centered on the bisector of the two boundary lines (a)  $m_1 = m_2$  and (b)  $m_1 = M_{\min}$ . This strategy would increase the detection probability of the signals in the deemed parameter space without using more templates. Note that by placing the tiles above the  $\eta = 1/4$  line, in the first stage, we are actually searching more than the mass range of  $1.0 - 30.0 M_{\odot}$ , because the tiles span a region which correspond to actual physical values of the individual masses but outside this range. If we include this region in our parameter space, then because the rectangles efficiently tile

the total space - by definition - the gain factor could rise above 100.

A search code for implementing the EHS algorithm is being written using the LIGO Algorithm Library (LAL) [14] for the LIGO Data Analysis System (LDAS) [15]. It is to be noted that the existing LAL implementation of the template bank generation is based on the quadratic approximation of  $\mathcal{H}$ . This is not suitable for the trigger stage of EHS which uses  $\Gamma$  ( $\simeq 0.82$ ). At these values of  $\Gamma$ , the quadratic approximation to the ambiguity function is no more adequate - which means that it is not feasible to use the metric formalism [25] to place trigger stage templates in the EHS scheme. Therefore, we plan to implement the approach of laying out the trigger stage templates using the algorithm described in this paper. The fine-bank templates will be layed out using the LAL bank package.

For each event detected in the first layer of the hierarchy, the *approximate* time of arrival  $t_a$  is already determined. Thus, only a smaller segment of the data at full sampling rate  $f_{\text{samp}}^{(2)}$  needs to be processed in the second stage. This could provide further savings in the second stage cost. However, as can be seen from Table III, most of the computational cost is incurred in the trigger stage, so that the improvement in speed-up factor will be small.

We have not addressed the issue of non-Gaussianity in this paper. However we believe that tail features would lead to higher false alarm rates in the trigger stage - necessiating an upward revision of the  $\Gamma_{\text{opt}}$  from present values of  $\sim 0.82$ . This would lead to a reduction in the computational advantage of the EHS method as more templates would be needed at this stage. But perhaps putting another sieve in between the hierarchy layers may alleviate the problem.

### Acknowledgments

The authors thank B.S. Sathyaprakash, S.D. Mohanty and P. Shawhan for useful discussions. A.S. Sengupta thanks LIGO Laboratory for a three month visit to LIGO Caltech and CSIR (India) for Senior Research Fellowship. S. Dhurandhar thanks Caltech for a visit during which writing of this paper was completed. The LIGO Laboratory works under cooperative agreement PHY-0107417. This work was partially funded under NSF grant INT-0138459. S. Dhurandhar and A. Lazzarini thank DST (India) and NSF (US) for the Indo-US collaborative programme. This document has been assigned LIGO Laboratory

- [1] R. A. Hulse and J. H. Taylor, *Ap. J.* **324**, 355 (1975).
- [2] J. H. Taylor, *Rev. Mod. Phys.* **66**, 711 (1994).
- [3] Abramovici, A., Althouse, W.E., Drever, R.W.P., Gürsel, Y., Kanwamura, S., Raab, F.J. Shoemaker, D., Sievers, L., Spero, R.E., Thorne, K.S., Vogt, R.E., Weiss, R., Whitcomb, S.E., and Zucker, Z.E., *Sciences* **256**, 325, (1992).
- [4] Danzmann K et al. in First Edoardo Amaldi Conference on Gravitational Wave Experiments (Ed. E Coccia, G Pizzella, F Ronga) (Singapore: World Scientific, 1995) p. 100
- [5] Tsubona, K., , in "300-m Laser Interferometer Gravitational Wave Detector (TAMA300) in Japan", in Coccia, E. Piaaella, G., Ronga, F. eds., *Gravitational Wave Experiments*, World Scientific, Singapore, 1995, p. 112-114.
- [6] Bradaschia, C., et al., *Nucl. Instrum. Methods Phys. Res. A*, **289**, 518 (1990).
- [7] K. S. Thorne, *Gravitational radiation: A new window onto the Universe*, gr-qc/9704042.
- [8] R. Weiss, *Rev. of Mod. Phys.* **71**(2), S187 (1999).
- [9] L. Blanchet, T. Damour, B.R. Iyer, C.M. Will and A.G. Wiseman *Phys. Rev. Lett.* **74**, 3515 (1995).
- [10] C. Cutler and K.S. Thorne, *An overview of gravitational wave sources*, gr-qc/0204090.
- [11] S.V. Dhurandhar and B.S. Sathyaprakash, *Phys. Rev. D* **49**, 1707 (1994).
- [12] B.S. Sathyaprakash and S.V. Dhurandhar, *Phys. Rev. D* **44**, 3819 (1991).
- [13] B. Allen *et. al.*, *GRASP: a data analysis package for gravitational wave detection*, Version 1.9.8. Manual and package available at <http://www.lsc-group.uwm.edu/>.
- [14] *LIGO/LSC Algorithm Library (LAL) Software Documentation*, available at <http://www.lsc-group.phys.uwm.edu/lal/>.
- [15] *LIGO Data Analysis System (LDAS) Software Documentation*, available at <http://www.ldas-dev.ligo.caltech.edu/doc/>.
- [16] G.M. Amdahl, Proc. of AFIPS Conference, Reston, VA, (1967).
- [17] B. Allen, J.K. Blackburn, P.R. Brady *et. al.*, *Phys.Rev.Lett.* **83**, 1498 (1999).
- [18] H. Tagoshi, N. Kanda, T. Tanaka *et. al.*, *Phys.Rev. D* **63**, 062001 (2001).
- [19] T. Tanaka and H. Tagoshi, *Phys.Rev. D* **62**, 082001 (2001).



- [20] F.A. Jenet and T.A. Prince, Phys.Rev. D **62**, 122001 (2000).
- [21] P.R. Brady, T. Creighton, C. Cutler and B.F. Schutz, Phys.Rev. D **57**, 2101 (1998).
- [22] E.K. Porter, gr-qc/0203020.
- [23] A. Buonanno, Y. Chen, M. Vallisneri, gr-qc/0211087, gr-qc/0205122.
- [24] A.S. Sengupta, S.V. Dhurandhar, A. Lazzarini and T. Prince, Class. Quantum Grav. **19** No 7, 1507 (2002).
- [25] B.J. Owen, Phys. Rev. D **53**, 6749 (1996).
- [26] B.J. Owen and B.S. Sathyaprakash, Phys. Rev. D **60**, 2002 (1999).
- [27] B.J. Owen, “*Problems in searching for spinning black hole binaries*”, GWDAW, Louisiana State University, (2000). <http://gravity.phys.lsu.edu/gwdaw/talks.html>
- [28] S. V. Dhurandhar and B. F. Schutz, Phys. Rev. D **50**, 2390 (1994).
- [29] S.D. Mohanty and S.V. Dhurandhar, Phys. Rev. D **54**, 7108 (1996).
- [30] S.D. Mohanty, Phys. Rev. D **57**, 630 (1998).
- [31] R.P. Croce, Th. Demma, V. Pierro and I.M. Pinto, Phys.Rev. D **65**, 102003 (2002).
- [32] The noise curves for the LIGO I target sensitivity curve are defined in LIGO technical publication E950018, ”LIGO Science Requirements Document”, <http://www.ligo.caltech.edu/docs/E/E950018-01.pdf>. The data are available from the LIGO Laboratory sensitivity curves archive site [http://www.ligo.caltech.edu/~lazz/LSC\\_Data](http://www.ligo.caltech.edu/~lazz/LSC_Data).
- [33] In much of recent literature as also in the LIGO Algorithms Library documentation [14], the square root in (2.8) is not taken. We however, choose to take the square root to facilitate computation of detection and false alarm probabilities. See III A for a discussion.